Clustering of H_2 molecules encapsulated in fullerene structures

R. E. Barajas-Barraza[1] and R. A. Guirado-López[1,2]
[1]*Instituto de Física "Manuel Sandoval Vallarta," Universidad Autónoma de San Luis Potosí, 78000 San Luis Potosí, México*
[2]*Programa de Ingenieria Molecular, Instituto Mexicano del Petroleo, Lazaro Cardenas 152, 07730, México D.F., México*
(Received 13 June 2002; revised manuscript received 15 August 2002; published 29 October 2002)

We have performed semiempirical (MNDO) as well as *ab initio* density-functional theory calculations at $T=0$ to analyze the hydrogen storage behavior in spheroidal C_{60} and C_{82}, and cylindrical finite-length (5,5) armchair C and BN fullerenes. We have found that, while chemisorption of individual H atoms to the external surface of the fullerenes is observed, hydrogen atoms cannot be attached to the inner wall of the structures and can only exist in a molecular form inside the fullerenes. We further find that, as a function of the symmetry of the encapsulating cavity and a delicate balance between repulsive energies among H_2 molecules inside the structures and those between H_2 molecules and the fullerene walls, molecular $(H_2)_N$ clusters of well defined shape are formed namely: linear configurations, two-dimensional zig-zag and triangular arrays, and three-dimensional structures such as octahedral and icosahedral clusters, as well as helicoidal cylindrical-shape assemblies. In the cylindrical configurations (C and BN tubes), hydrogen atoms are placed inside the structures up to a bond breakage of the fullerene network, which allow us to estimate the maximum storage capacities of the different configurations. Actually, in our closed nanotubes, we relate the bond breakage mechanism to the development of a nonuniform hydrogen accommodation along the tubes, driven by the both highly anisotropic H_2-H_2 and wall-H_2 repulsive interactions. With increasing the number of stored H_2, tubes are found to be mainly radially deformed, a fact that reduces (up to $\sim$13%) the energy difference between the highest occupied and lowest unoccupied molecular orbitals in the structures. Finally, saturation of the tube ends with molecular terminations results in stable compounds from which a density-controlled storage of hydrogen seems to be possible.

DOI: 10.1103/PhysRevB.66.155426 PACS number(s): 61.48.+c, 72.80.Rj

I. INTRODUCTION

Fullerene related materials have attracted considerable attention this last decade due to their unique physical and chemical properties. Compared to other carbon structures, fullerenes have revealed promising applications in a wide variety of very important technological processes such as in designing electronic devices, superfibers, catalytic materials, etc. Apart from considerable efforts to understand their formation process,[1] particular attention has been also given to the type of materials that can be obtained by doping them with heavy atoms or with different kind of molecules.[2] One of the most striking results in this respect corresponds to the alkali-doped C_{60} compounds which display superconductivity at reasonable high temperature[3] and very recently, applications as magnetic detectors and in magnetic recording technology are being envisioned.[4] In addition, their large empty space (particularly inside carbon nanotubes), has open also new applications as storage materials with high capacity and stability. These cavities are large enough to accommodate a wide variety of atomic and molecular species, the presence of which can significantly influence the properties of the material. In particular, the storage of hydrogen in single-wall nanotubes (SWNT's) has attracted much experimental and theoretical interest,[5] being their use in fuel cells for power generation one of the most promising applications.

In the past years, different experimental measurements have been performed in order to determine the maximum hydrogen storage capacity in several carbon compounds. For example, crystalline fcc C_{60} has been observed to absorb H_2 in octahedral interstices, providing a small storage capacity of only 0.28 wt % at 40 °C.[6] Recently, Dillon *et al.*[7] reported that hydrogen could be stored in bundles of SWNT's up to 5%–10%, where H_2 molecules are physisorbed at the exterior surfaces or located between the interstitial spaces separating the tubes. Moreover, Chambers *et al.*[8] claimed to observe a remarkable large amount of hydrogen (67 wt. %) adsorbed on graphite nanophibers for pressures of about 100 atm and temperatures around 300 K. These last two reported capacities, in particular, are higher than any observed before for known types of carbon materials and actually, they have not been corroborated in any other theoretical[9] or experimental investigation of hydrogen adsorption on nanofibers[10] and carbon nanotubes.[11]

Until now, the most useful method for storage of hydrogen in an array of SWNT's was thought to be physisorption on the outer surface or in the interstices between nanotubes.[12] However, the desorption behavior for physisorbed hydrogen may limit its applications in the field, where stable storage of hydrogen in the SWNT sample would be required at temperatures considerably higher than room temperature. On the other hand, it is also possible to fill SWNT's with H_2 by capillarity,[13] or by performing collisions between hydrogen atoms and SWNT's.[14,15] Concerning the latter technique, many results using energetic collisions between fullerenes and various atoms, molecules, or ions to form endohedral complexes have been reported[16] and, despite bond breakage and subsequent cage destruction can be induced, in the particular case of SWNT's, their superior mechanical strength and capacity of broken bond recovery at room temperature can be used to surmount the storage density obtained by capillarity to a super high density.

From the theoretical point of view, there are several studies (at different levels of approximation) in which adsorption

and insertion of hydrogen on an array or in isolated SWNT's have been performed.[15,17,18] Encapsulation or adsorption to the external surface of nanotubes with different diameters, or separated by various distances (in the case of periodic arrays) have been considered, and important details concerning the hydrogen adsorption sites, their stability, and electronic properties have been obtained. In particular, from these studies it is clear that a large amount of H_2 molecules can be trapped inside SWNT's, and that the hydrogen storage capacity is limited by the repulsive interactions between H_2 molecules and those between H_2 molecules and the fullerene wall.[18] Furthermore, by considering charged nanotubes, recent theoretical studies[19] have found a significantly better performance for hydrogen storage, increasing the adsorption as 10%–20% at 298 K with respect to uncharged SWNT's systems.

However, despite all this intense research activity, little attention has been paid to the different condensed phases of hydrogen molecules that could be induced in such confined environments and that, as will be seen in the following, are of crucial importance (particularly at high densities) in determining the stability and maximum storage capacity of carbon nanotubes. At this point, it is important to comment that previous molecular dynamics studies on H_2 molecules encapsulated in a SWNT have already reported the formation of a molecular assembly of cylindrical shape.[15] Furthermore, as a function of the density of stored hydrogen and the tube radius Lee and Lee.[18] observed, through density-functional theory (DFT) calculations, a large variety of coaxial molecular configurations, playing the repulsive interactions among the different atomic species involved a key role in their formation and stability. Interesting related condensed-phase monolayer films have been also found in rare gas and hydrogen films adsorbed on the inner surfaces of carbon nanotubes[20] and finally, Hodak and Girifalco[21] have applied a lattice gas Hamiltonian to analyze the structural properties of C_{60} molecules encapsulated in open and closed (10,10) nanotubes and, in agreement with high-resolution transmission electron microscopy observations, they have found the formation of an almost perfect one-dimensional C_{60} molecular solid. Moreover, for closed tubes at room temperature, they have obtained a broad distribution of $(C_{60})_N$ clusters, their sizes decreasing with increasing the temperature of the system.

In this work, we have carried out semiempirical and *ab initio* DFT calculations for several H_2 molecules encapsulated in various carbon fullerene structures (spheroidal C_{60} and C_{82} as well as in cylindrical C_{110}) in order to analyze the form of stored hydrogens and to find out the maximum storage capacities of the different configurations. Our calculations give a detailed description on the formation of several molecular H_2 clusters of different sizes and geometries, the latters being mainly determined by the symmetry of the encapsulating cavity. Furthermore, we analyze the hydrogen storage behavior in a cylindrical 110-atom BN fullerene which, even if it has approximately the same dimensions than the corresponding carbon arrangement, the different nature of the B—N chemical bonds could increase (decrease) the density of stored hydrogens. This last case is important to analyze since single-wall BN nanotubes and related fullerene structures (multiwall nanotubes, bundles, etc.)[22] have also shown remarkable stability, being their hydrogen storage capacity still previously unexplored. Finally, in view of possible applications and to see also the influence of the capped ends, hydrogen storage in a carbon nanotube capped with organic molecules is also analyzed.

The rest of the paper is organized as follows. In Sec. II we briefly describe the theoretical models used for the calculations. In Sec. III we present our results and finally, in Sec. IV the summary and conclusions are given.

II. METHOD OF CALCULATION

The number of atoms involved in our considered systems (up to ~ 200) limits the applicability of density-functional (DF) optimization-based methods and that is why we have decided to perform our systematic study by combining two different theoretical approaches. In a first step, we have fully optimized the considered structures using the semiempirical modified-neglect-of-diatomic-overlap (MNDO) level of theory[23] and then, in a second step, we have used these MNDO geometries to perform single-point DF calculations considering the Becke exchange functional and the Lee-Yang-Parr correlation.[24]

This procedure could be justified since the accuracy of the MNDO method has been proved in several calculations of fullerenes and fullerene-derived materials. For example, for the C_{60} molecule MNDO finds bond lengths of 1.474 and 1.400 Å,[25] for single and double bonds respectively, in good agreement with gas phase electron studies (1.458 ± 0.006 Å and 1.401 ± 0.010 Å)[26] and *ab initio* calculations (1.446 Å and 1.406 Å).[27] In the case of a fully relaxed (5,5) armchair carbon nanotube we obtain a diameter of 6.9 Å with an average nearest-neighbor bond length of ~ 1.44 Å, both quantities being almost the same than that reported with more elaborated calculations.[18] MNDO calculates the ionization potential of C_{60} to 8.95 eV,[25] slightly larger than the values obtained from *ab initio* calculations[28] (7.92 eV) and experiment[29] (7.56–7.62 eV) and finally, doped fullerenes[30] [e.g., Li_xC_{60} $(x=0 \ldots 14)$] and large carbon clusters[25,31] have also been successfully studied using the MNDO approximation.

It is important to comment that MNDO theory gives also a very good estimation for the C-H distance and angular H-C-H distribution in several carbon-hydrogen compounds. For example, for the interaction of H with the external surface of a C_{60} we obtain that hydrogen is chemisorbed on top of a C atom of the cage with a C—H bond length of 1.11 Å. In the case of methane, a tetrahedral structure is found with a H-C-H angle of 109.4° and a C—H bond length of 1.10 Å. In fact, for an extensive comparison between MNDO theory and experimental results, and also with more elaborated quantum chemical calculations (e.g., heats of formation, molecular geometries, rotational barriers, bond lengths, etc.), the reader is referred to the Ref. 23.

The electronic structure and total energy of the molecules are obtained by means of the GAUSSIAN98 software,[32] where the molecular orbitals are expanded as a combination of

Gaussian functions centered at the atomic sites, and the exchange correlation effects can be treated within the density-functional scheme. In particular, the Kohn-Sham equations are solved by considering the nonlocal Becke exchange functional and the Lee-Yang-Parr correlation (BLYP).[24] We use the slater-type orbitals (STO)-3G basis[33] which is a minimal set that is formed by fixed-size atomic-type orbitals. The STO−3G considers three Gaussians per basis function, for example, in a carbon atom we have three gaussians which are a least-square fit to a Slater 1*s* orbital, and we have also another three Gaussians which are a least-square fit to Slater 2*s* and 2*p* orbitals. Obviously, larger basis sets approximate more accurately the orbitals by imposing fewer restrictions on the location of electrons in space. As a consequence, in order to illustrate the dependence of results on the choice of basis functions, we have done some calculations by using a more extended set, 6−21G.[34] The calculations, which involved a higher numerical effort, are found to lead essentially to the same conclusions.

The numerical accuracy of the method is tested by calculating some well-known properties of the C_{60} molecule. We obtain, by using the minimal STO-3G basis set, that the occupied electronic states fall within a range of 19.2 eV and that the energy difference between the highest occupied molecular orbital (HOMO) and lowest unoccupied molecular orbital (LUMO) is of 1.45 eV, both results being in good agreement with the calculations of Kobayashi and Morita based on the nonlocal DFT with generalized-gradient approximation (GGA).[35] On the other hand, we must say that our values are underestimated when compared with experimental measurements performed on C_{60} thin films (HOMO-LUMO energy gap of 2.3 eV and valence-band width of 23 eV),[36,37] where solid-state effects like ordering of the molecules and shrinkage of the cluster lattice are known to produce sizable modifications in the electronic spectra. We found, for the C_{60} molecule, an atomization energy of 10.04 eV/at which is overestimated with respect to the reported values in the literature, however, as clearly stated by other authors,[38] this corresponds to a basis set effect. Actually, the calculation using the 6−21G basis gives an atomization energy of 8.56 eV/at, which is closer to the estimated experimental value of 7.25 eV/at.[39] Therefore, in the following, only relative values are important.

For our fully relaxed 110-atom (5,5) armchair carbon tube we calculate, at the STO-3G level, an HOMO-LUMO energy gap of 0.14 eV, which clearly reflects the conducting properties of these structures. In addition, the chemical adsorption of a single H atom on the external surface of a (5,5) nanotube is also found with an adsorption energy of 3.31 eV. However, by using the more extended 6−21G basis set we obtain a value of 1.09 eV, being in good agreement with molecular dynamics simulations[15] (1.19 eV) in which both the energetics and the geometrical degrees of freedom are treated on the same theoretical level. Finally, and in sharp contrast to the corresponding pure carbon structure we found, for our fully relaxed 110-atom BN tube (of $\sim$7.2 Å in diameter), an HOMO-LUMO energy gap of 3.4 eV which clearly reflects the well-known semiconducting character of these structures. We must comment that this calculated value for the energy gap is reduced when compared with the ones obtained for BN tubes with larger diameters ($\sim$5 eV for tubes with radii $\geqslant$6 Å), however, this could be reasonable to expect since it has been demonstrated by Rubio *et al.*[40] that, in BN tubes, the band gap increases with diameter, rapidly saturating at the hexagonal BN value. In fact, it is important to comment that energy gaps of the order of 3 eV have been also found in Ref. 40 when considering BN tubes with similar dimensions (chiralities) than the one considered in our work. These findings together with the previous results on pure carbon structures demonstrate that our hybrid approach well describes the energetics and the local electronic structure of our considered fullerenes compounds.

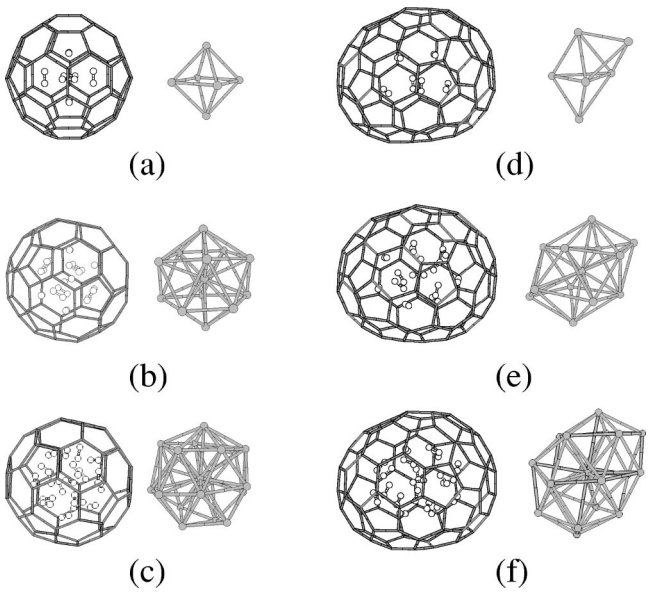

FIG. 1. Calculated (MNDO) lowest-energy structures (first and third columns) together with the spatial distribution of the center of masses of the encapsulated hydrogens (second and fourth columns) for (a) $(H_2)_6@C_{60}$, (b) $(H_2)_{13}@C_{60}$, (c) $(H_2)_{19}@C_{60}$, (d) $(H_2)_6@C_{82}$, (e) $(H_2)_{13}@C_{82}$, and (f) $(H_2)_{19}@C_{82}$ fullerenes.

III. RESULTS AND DISCUSSION

A. Hydrogen encapsulation in spheroidal C_{60} and C_{82}

Despite hydrogen encapsulation in relatively small spheroidal fullerene molecules is probably not as important for gas storage applications as is the case in carbon nanotubes, it is for sure very useful in order to get a physical insight into the structural properties of small molecules encapsulated in such confined environments. In Fig. 1 we show as representative results the MNDO equilibrium configurations for 6, 13, and 19 H_2 molecules encapsulated in spheroidal C_{60} [Figs. 1(a), 1(b), and 1(c)] and C_{82} [Figs. 1(d), 1(e), and 1(f)]. The number of internal molecules studied ranges from 1 to 23 for C_{60}, and from 1 to 35 for C_{82}, the latters defining the maximum storage capacity for each one of the carbon fullerenes.

The equilibrium structures shown in Fig. 1 were calculated by computing the force at each atomic site and relaxing the geometry, without symmetry constraints, by the method

of steepest descent. Different starting configurations were used (e.g., disordered arrangements of diatomic molecules as well as randomly distributed isolated H species) to ensure that the geometry of the molecule corresponds to the global minimum. From the figure we can see that, in all cases, the encapsulated hydrogens only exists in a molecular form (H_2) inside the fullerenes and that do not adsorb to the internal surface of the carbon structure. In all cases we found H—H bond lengths of 0.66 Å (obviously underestimated by the semiempirical approximation), being actually the same than the MNDO value obtained for the isolated H_2 case.[23] On the other hand, the various C—C bonds in both cages are gradually expanded as a function of the number of stored hydrogens reaching, at the highest density, an average nearest-neighbor C—C bond of 1.56 and 1.54 Å for C_{60} and C_{82}, respectively, being in fact comparable with the measured C—C bonds of diamond (1.53 Å). We must comment that these results are in qualitative agreement with the DFT studies performed by authors of Ref. 18 addressing the effective hydrogen storage in SWNT's. These authors have considered an initial configuration consisting of individual hydrogen atoms adsorbed at the internal surface of a nanotube, configuration that has been found to be unstable after full relaxation of the system, resulting only in the formation of H_2 molecules having also H—H bonds very close to the DFT value obtained in the isolated case (0.75 Å). Furthermore, for relatively high H_2 density uptakes, values of $\sim$1.52 Å are also observed between the various nearest-neighbors C—C bonds of their cylindrical cavities, being of the order of the ones found in our spheroidal fullerenes at high hydrogen concentration regimes. From these results it is thus evident that repulsive interactions among the encapsulated hydrogens and the fullerene wall, as well as between the various H_2 molecules formed are present, and play an important role for determining the hydrogen storage capacity in these hollow carbon structures.

From our calculations we have found that, besides the repulsive interactions present in the systems, there are also some confinement effects that are of crucial importance in determining the ground-state structure and stability of these compounds. This is inferred from Figs. 1 and 2 where actually both effects are combined to induce the formation of various H_2 molecular clusters of well-defined shape. In order to see this more clearly, we have decided to plot at the right of each $(H_2)_N@C_{60(82)}$ equilibrium configuration the position of the molecular centers of mass of the encapsulated hydrogen molecules. We note that 6 [Fig. 1(a)] and 13 [Fig. 1(b)] H_2 molecules inside the C_{60} fullerene arrange themselves in well-defined configurations, namely, octahedral and icosahedral clusters. However, for 19 H_2 molecules [Fig. 1(c)] (which defines a relatively large density of encapsulated hydrogen for the C_{60} cavity), a considerable distorted ''icosahedral-like'' structure is found, defining a kind of ordered-disordered structural transition as a function of the number of stored hydrogens. We must comment that similar structural rearrangements have been obtained when analyzing the equilibrium geometry and thermodynamics of $(CO_2)_N$ (Ref. 41) and $(SF_6)_N$ (Ref. 42) molecular clusters where, as a function of *N*, noncrystalline (icosahedral-like) to crystalline (cubic) structural phase transitions are observed. It is important to remark that, in all our geometry optimizations, disordered arrangements were always assumed as initial configurations, however, they turned to be unstable after switching on the minimization procedure, gradually evolving to the highly symmetric structures shown in the figures.

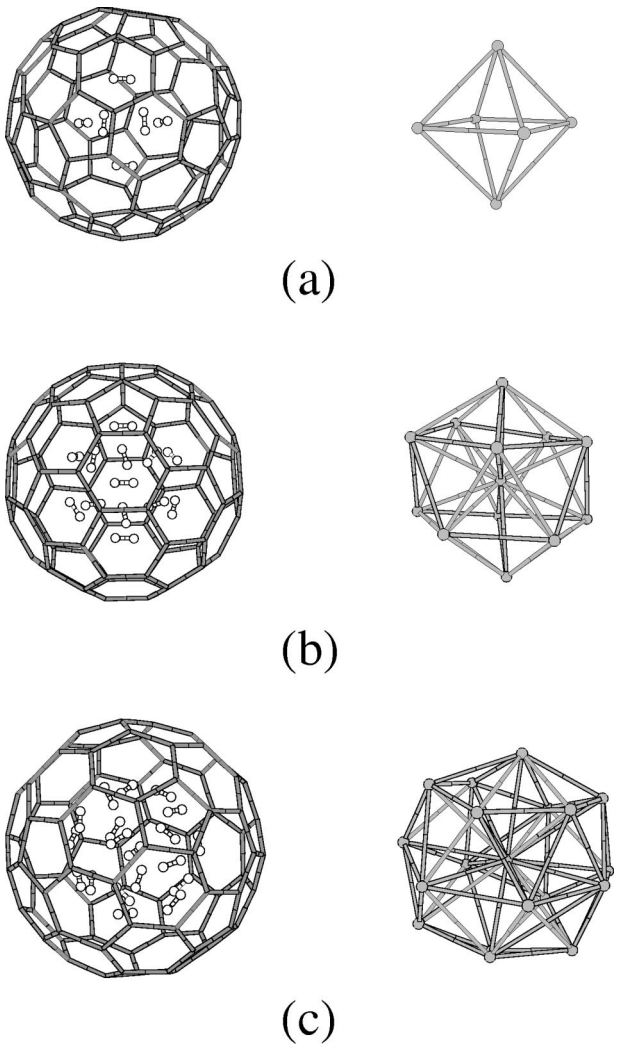

FIG. 2. Calculated (MNDO) lowest-energy structures (left column) together with the spatial distribution of the center of masses of the encapsulated hydrogens (right column) for (a) $(H_2)_6@C_{82}^{I}$, (b) $(H_2)_{13}@C_{82}^{I}$, and (c) $(H_2)_{19}@C_{82}^{I}$ fullerenes.

In order to analyze the influence of the size and symmetry of the encapsulating cavity on the equilibrium geometry of the endohedral molecular H_2 clusters we present also in Fig. 1 results for 6 [Fig. 1(d)], 13 [Fig. 1(e)], and 19 [Fig. 1(f)] H_2 molecules encapsulated in a low-symmetry C_{82} isomer. From the figure we can see that, when compared to the results obtained for the C_{60} cavity, the equilibrium geometry of the $(H_2)_6$ cluster suffers a structural transformation [compare Figs. 1(a) and 1(d)], being now characterized by a less coordinated arrangement (single-capped trigonal bipyramid). Moreover we note that, for this sequence, distorted configurations are already present for $(H_2)_{13}$ [compare Figs. 1(b) and 1(e)], both facts reflecting the crucial role played by the precise geometrical details of the encapsulating cavity on the

global structure of the guest molecules. Actually, if we consider a more spherical C_{82}^{I} isomer (see Fig. 2), we clearly see again the formation of well-ordered octahedral and icosahedral-like clusters for $N=6$ and 13 H_2 molecules, being almost the same that the ones found inside the 60-atom fullerene. These results could be of fundamental importance when encapsulating magnetic guests (for which applications in magnetic recording technology are being envisioned), since it is well known that, in magnetic systems, small changes in their local atomic environment can lead to significant variations in their magnetic properties.

It is important to note that the ordered→disordered structural transitions found in Figs. 1 and 2 as a function of the stored hydrogens goes in hand with the correlated →uncorrelated molecular orientation transitions also present in the molecular clusters. As is well known, many bulk systems consisting of highly symmetric molecules change their structure at a phase transition as a result of orientation ordering or disordering of the molecules.[43] This fact is also clearly seen from the sequence shown in Figs. 1(a), 1(b), and 1(c) where we note that, besides the symmetrical positions adopted by the center of masses of 6 (O_h) [Fig. 1(a)] and 13 (I_h) [Fig. 1(b)] H_2 molecules, correlated orientations between the various molecular axes are also observed. Thus the clusters are orientationally and translationally ordered. However, note that the lattice distortions that deviates the $(H_2)_{19}$ cluster geometry [Fig. 1(c)] from the ideal icosahedral packing are coupled to a rotational phase transition (characterized by a randomly oriented molecular configuration) obtained also for that number of encapsulated hydrogens. Reorientations of H_2 molecules (leading to disordered arrays) are accompanied then by considerable distortions of the cluster lattice, a fact that clearly reveals the strong coupling between orientational and translational order in real systems, depending thus the interaction potential in molecular clusters not only on the positions of the molecules but also on their relative orientations.

We have checked the reliability of our structural optimizations by comparing our equilibrium geometry found for the $(H_2)_6@C_{60}$ fullerene [Fig. 1(a)], with the ones obtained by means of *ab initio* Hartree-Fock and DFT-(LDA) local-density approximation calculations. Within the HF and DFT approaches, in which obviously the interatomic potential is gradually more accurately described, the structures obtained do not differ significantly from the one optimized at the MNDO level (all three belonging to the O_h symmetry), the main differences lying in the larger H_2-H_2 distances (up to 2%) found in the more accurate theories.

Finally, in Fig. 3, we present results for the intercalation energy per atom, E_{int}, of the C_{60} and C_{82} fullerenes as a function of the number of stored hydrogens defined as

$$E_{int}=[E_t[(H_2)_N@C_{60(82)}]-NE_t(H_2)-E_t(C_{60(82)})]/N_{\mathrm{at}}, \tag{3.1}$$

where $E_t[(H_2)_N@C_{60(82)}]$ is the total energy of the hydrogen-containing fullerenes, $E_t(H_2)$ and $E_t(C_{60(82)})$ are the total energies of single gaseous H_2 and $C_{60(82)}$ molecules, and $N_{\mathrm{at}}(N)$ define the total number of atoms (H_2 molecules) in the structure. According to this definition (where all total energies are negative), a stable system will have a negative value for the intercalation energy. From the figure we can see thus that it is already quite challenging to incorporate a few H_2 molecules inside both C_{60} and C_{82} cavities, clearly reflecting the strong repulsive interactions between the different chemical species present in the system. At this respect, it is important to comment that despite our total-energy calculations have demonstrated that endohedral $(H_2)_N@C_{60(82)}$ fullerenes will be difficult to isolate it could be possible that, by performing low-energy H-ion bombardment on a C_{60} sample, H atoms may get trapped in the fullerene cage.

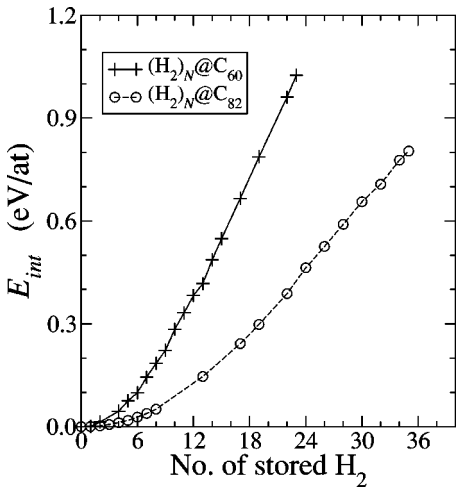

FIG. 3. The intercalation energy E_{int} per atom for $(H_2)_N@C_{60}$ and $(H_2)_N@C_{82}$ fullerenes as a function of the number of encapsulated hydrogens.

As a conclusion of this section we would like to comment that the various physical trends shown in the figures, and which in fact have been also observed for similar related systems, can lead us to conclude that within our theoretical framework and model system (carbon cages + diatomic molecules) we are able to describe, at least qualitatively, realistic phenomena of molecular systems in confined environments. We would like to add finally that the motivation of this section has been primarily scientific, and we think that a number of new insights into the behavior of small molecules encapsulated in fullerene structures has been obtained.

B. Hydrogen storage in tubelike arrangements

We turn now to the most interesting case concerning the hydrogen storage in tubelike arrangements. Although most previous theoretical works on hydrogen storage have primarily dealt with infinite-length nanotubes on account of the simplification offered in various of the formalisms it is well known that, as produced tubes could be capped, among other ways, with hemispherical fullerene domes containing six pentagons required to produce closure. Obviously, the use of this type of boundaries should strongly influence the equilibrium filling when compared to the one obtained using periodic conditions, being thus a key issue that must be also considered when analyzing the hydrogen storage capacity in real nanotubes compounds.

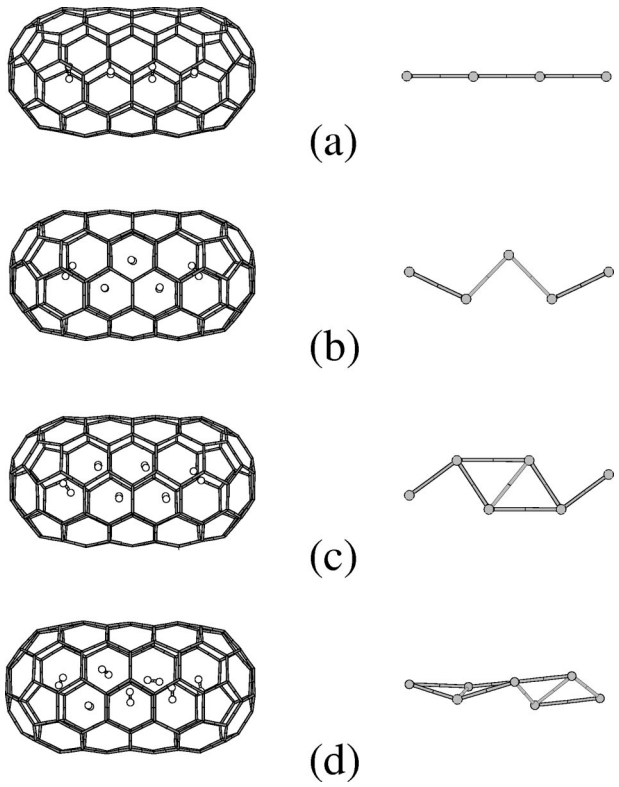

FIG. 4. Calculated (MNDO) lowest-energy structures (left column) together with the respective spatial distribution of the center of masses of the encapsulated hydrogens (right column) for (a) $(H_2)_4@C_{110}$, (b) $(H_2)_5@C_{110}$, (c) $(H_2)_6@C_{110}$, and (d) $(H_2)_7@C_{110}$ fullerenes.

In our cylindrical structures, the number of encapsulated H_2 molecules goes from 1 to 40 for C_{110} and from 1 to 41 for the $B_{55}N_{55}$ tube, the latters defining the maximum storage capacity for each one of the encapsulating cavities. In this case, we use also the MNDO Hamiltonian to perform full symmetry unconstrained relaxations since, as already seen in the preceding section, the repulsive interactions between fullerene walls and hydrogen is fairly strong and can give raise to sizable deformations of the encapsulating cavity, being obviously of crucial importance for determining the stability and equilibrium properties of these compounds. Although it is desirable to have the calculations performed self-consistently on the *ab initio* level, the size of the system makes this prohibitively expensive and it is thus necessary to accept approximations.

1. Hydrogen storage in a (5,5) C_{110} *capsule*

In Figs. 4 and 5 we show as representative results our equilibrium structures found for 4, 5, 6, 7 (Fig. 4), and 18, 30, 40 (Fig. 5) H_2 molecules encapsulated in a C_{110} tubelike arrangement. Furthermore, as in the last section, we show also the position of the center of mass of each one of the encapsulated hydrogens molecules, together with a side view (see second column of Fig. 5) of the equilibrium structures obtained. The configurations plotted in the figures were chosen because they clearly reveal (as in the last section) the wide variety of structural transitions (both translationally and orientationally) present in the system as a function of the number of stored hydrogens.

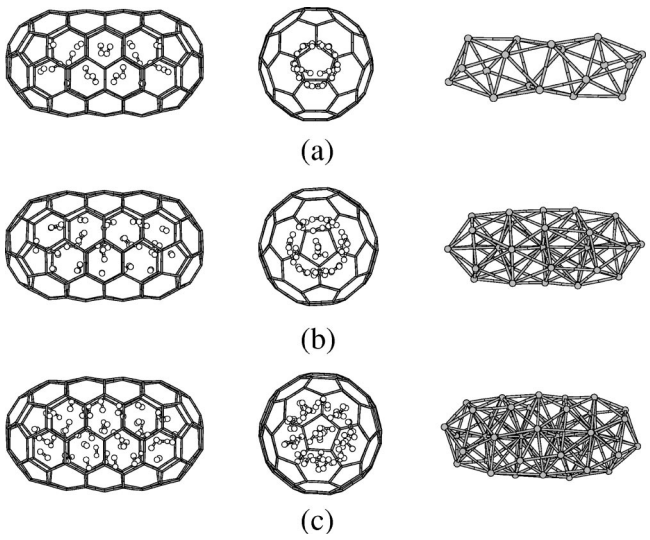

FIG. 5. Calculated (MNDO) lowest-energy structures (left column), side-view of the equilibium configurations (central column), and the respective spatial distribution of the center of masses of the encapsulated hydrogens (right column) for (a) $(H_2)_{18}@C_{110}$, (b) $(H_2)_{30}@C_{110}$, and (c) $(H_2)_{40}@C_{110}$ fullerenes.

From Fig. 4(a) we can see that 4 H_2 molecules arrange themselves inside the C_{110} fullerene in a perfect one-dimensional structure, and in which it is possible to appreciate also a well-defined orientational ordering of the various molecular axes. One-dimensional arrays of H_2 molecules have been also obtained in grand canonical Monte Carlo molecular simulations when placing H_2 molecules in the interstitial space between nanotubes with a small tube-tube separations (4 Å) and relatively small tube diameter (10 Å).[44] However, in this case, the structural parameters of the tube array artificially define a narrow space in which it is only possible to accommodate only a single column of tightly pack hydrogen molecules. For 5 H_2 [Fig. 4(b)], a one-dimensional (1D)→two-dimensional (2D) structural transition is observed in which the guest molecules form now a ziz-zag array. This is due to the fact that the repulsive interactions with the capped ends do not allow anymore the one-dimensional growth sequence, allowing thus two-dimensional displacements of the encapsulated molecules. Moreover, note that this structural transformation is also coupled with a correlated reorientation of the various molecular axes. Adding one more hydrogen molecule to the system [Fig. 4(c)] results in a still very symmetrical 2D triangular array and finally, 7 H_2 molecules stabilize the first 3D structure [Fig. 4(d)], being formed by a kind of ''rombohedral-like'' twisted array in which, unlike in previous cases, disordered orientations of the molecules are now present.

In Fig. 5 we show similar results but for intermediate and large concentration regimes, namely, 18 [Fig. 5(a)], 30 [Fig. 5(b)], and 40 [Fig. 5(c)] H_2 molecules inside the C_{110} cavity. From Fig. 5(a) we can clearly see that 18 H_2 molecules con-

dense to a molecular shell with tube shape and which is characterized by a strongly correlated orientation of the various H_2 molecular axes. Furthermore we can also observe, by plotting the positions of the center of masses, that such orientational ordering leads to a global deformation of the molecular cluster as a whole, inducing more precisely the formation of an helicoidal cylindrical-shape assembly. In fact, we can think of this structure as being stabilized due to the transfer of the boundary conditions of the fullerene cavity to the encapsulated hydrogen, inducing thus structural phases in systems which do not themselves form tubelike arrangements. Similar results have been obtained by Ma *et al.*[15] by means of molecular dynamics simulations in which 90 hydrogen atoms encapsulated in a 150-atom finite-length (5,5) SWNT form a molecular assembly of cylindrical shape.

By increasing the number of encapsulated hydrogens we obtain additional structural transitions characterized mainly by the accommodation of H_2 species on the surface as well as at the interior of the molecular assembly. Actually, note that the hydrogens located inside the molecular cluster are always placed along the principal axis of the cylindrical cavity (z axis) [see Figs. 5(b) and 5(c)] forming again, as in the low concentration regime [see Fig. 4(a)], a perfect one-dimensional array $[1D@(H_2)_N@C_{110}]$. In this respect, our results differ from the ones obtained by Ma *et al.*[15] which, even at the highest densities, always obtain a hollow cylindrical molecular structure $[(H_2)_N@C_{150}]$. On the other hand, they agree with the DFT calculations performed by Lee and Lee.[18] which have observed, also inside a (5,5) SWNT, the formation of a molecular assembly of cylindrical shape with hydrogen molecules perfectly placed also along the principal axis of the encapsulating cavity. In addition, they have found that, by increasing the tube diameter, their equilibrium configurations evolve to the formation of various concentric cylindrical molecular assemblies.

It is important to comment that similar features as the ones shown in Fig. 5 have been observed in colloidal suspensions confined in cylindrical cavities,[46] where the analysis of the concentration profiles has revealed also that the particles are structured in cylindrical shells which occupy most of the available radial space. Furthermore, by looking the angular density distribution of the various molecular axes near the fullerene wall we have noted that our results also agree with grand canonical Monte Carlo simulations for N_2 and Br_2 molecules encapsulated in single-wall carbon nanotubes[45] which show that, in the low concentration regime, diatomic molecules adjacent to the wall prefer to orient parallel to the wall [see Figs. 5(a) and 5(b)] while, at higher densities, it is possible to observe the formation of a wall layer made up of a mixture of wall-parallel and wall-perpendicular configurations [see Fig. 5(c)].

At this point we would like to comment that a molecular crystal composed of nonspherical molecules at $T=0$ normally assumes an ordered arrangement of molecular axes, which together with the ordered spatial distribution of the center of masses of the molecules make the total energy of the system a minimum. However, by increasing the temperature, the alignment of molecular axes gradually becomes random due to the thermal motions, and eventually the low-temperature phase becomes unstable and the system suffers a structural phase transition. Form Figs. 4 and 5 it is clear that, in confined systems, and even at $T=0$, a kind of density-dependent breakdown of the correlated molecular orientations together with ordered→disordered displacive phase transitions can be also obtained.

As in the spheroidal fullerenes, we have found that hydrogen atoms cannot be attached to the inner wall of the structure and can only exist as H_2 molecules inside the tube. This result disagrees with the ground-state configuration obtained in Ref. 15 in which, of the 90 encapsulated H atoms (that define the maximum storage capacity in their 150-atom SWNT at room temperature), 86 atoms form 43 H_2 molecules, leaving two H atoms weakly bonded to the inner wall of the tube and the others as free H atoms inside the cavity. Within our theoretical framework, we have tried to induce the formation of a similar configuration in order to compare the energetics of the different forms of stored hydrogens. We have performed, for the highest H_2 uptake, additional calculations considering initial configurations consisting of 70 hydrogens in a diatomic state (H_2) together with 10 hydrogens as isolated atoms inside our C_{110} capsule. After several relaxations of the system, we have obtained a similar configuration to the one reported by Ma *et al.*, consisting of 74 atoms forming 37 H_2 molecules together with 6 H atoms weakly bonded to the inner wall of the carbon structure [we have found C—H bond lengths 4% larger when compared to the ones obtained in the exohedral adsorption (1.1 Å)]. However, when analyzing the relative stability between the equilibrium configuration shown in Fig. 5(c) [in which only diatomic molecules are present at the interior of the tube] with the one previously found (in which only the 7.5% of the encapsulated H atoms are present as isolated species) we have found and energy difference of 3.3 eV, being the latter arrangement considerable less stable.

At this respect, it is important to comment also that the intermolecular potential between H_2 molecules used in the simulation of Ma *et al.*[15] is spherical and thus independent of the relative orientation of the encapsulated hydrogens. By looking at our results shown in Figs. 1–5 it is clear that for diatomic molecules in confined environments this is not the case, and that sizable variations in the equilibrium filling and in the form of stored hydrogens can be obtained.

In order to describe the bond breakage mechanism of the fullerene wall, which defines the maximum storage capacity of the C_{110} capsule (being in our case of about 6 wt %), it is important to analyze the precise details of the distribution of the encapsulated H_2 molecules as well as the evolution of the various repulsive H_2-H_2 and wall-H_2 interactions present in the system as a function of the number of stored hydrogens. To see this more clearly, we plot first in Figs. 6 and 7 the distribution of axial distances of the center of masses of the encapsulated molecules with respect to the principal symmetry axis of the tube (z axis) for low, intermediate, and high concentration regimes. Furthermore, we show also in the insets of both figures the corresponding distribution of distances for each one of the carbon atoms of the cage, also with respect to the z axis, in order to analyze the kind of structural transformations induced in the encapsulating cav-

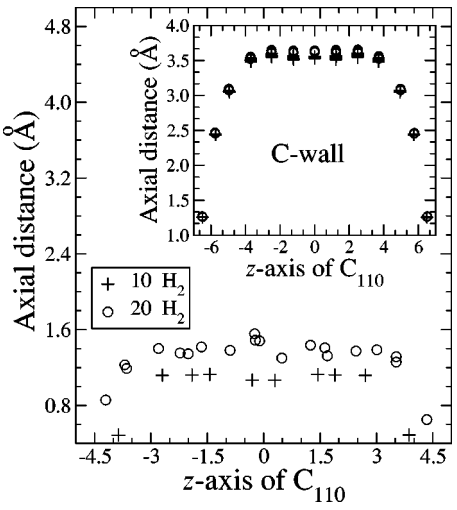

FIG. 6. Axial distance (in Å) of each one of the center of masses of the encapsulated H_2 in a C_{110} fullerene with respect to the principal symmetry axis of the cavity (z axis) for 10 H_2 (plus) and 20 H_2 (open circles). In the inset, we show similar results but for each one of the C atoms of the carbon capsule.

ity. From Fig. 6 we can clearly see that, for the low concentration regime (10 H_2), the hydrogen molecules are uniformly placed along the tube, being located approximately at 1.06 Å from the z axis. However, for 20 H_2, we can observe the development of a less uniform accommodation of encapsulated hydrogens, leading to the formation of a more defined parabolic distribution of molecules. Notice also from the inset that, for these two concentration regimes, only the positions of the carbon atoms located at the center of the tube are modified, suffering radial expansions of the order 3.5% with respect to the positions found in the empty structure. This result already reveals that the magnitude of the repulsive interactions of hydrogen with the capped ends differ

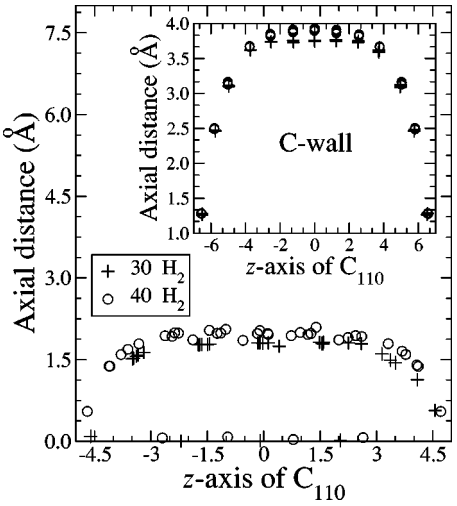

FIG. 7. Axial distance (in Å) of each one of the center of masses of the encapsulated H_2 in a C_{110} fullerene with respect to the principal symmetry axis of the cavity (z axis) for 30 H_2 (plus) and 40 H_2 (open circles). In the inset, we show similar results but for each one of the C atoms of the carbon capsule.

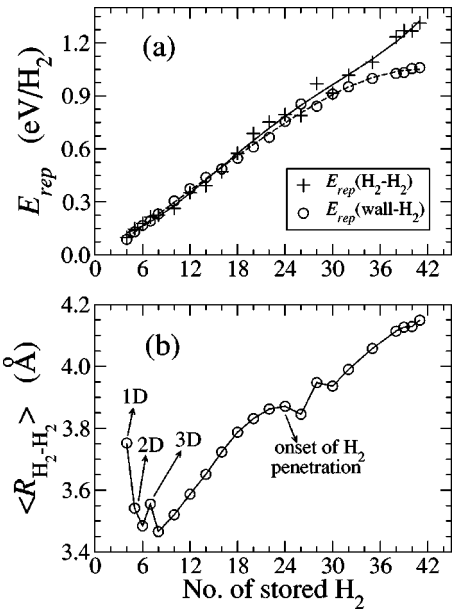

FIG. 8. (a) H_2-H_2 (plus) and wall-H_2 (open circles) repulsive energies as a function of the stored hydrogens in a C_{110} fullerene. (b) Average distance between the center of masses of the encapsulated hydrogens in a C_{110} fullerene.

from those between hydrogens and the central region of the tube, leading obviously to a highly nonuniform distribution of strain on the fullerene cavity.

From Fig. 7 we note that the positions of the encapsulated hydrogens, for both 30 and 40 H_2, clearly reflect the formation of cylindrical molecular assemblies as the ones shown in Fig. 5 (compare the hydrogen distribution profile with the one shown in the inset for C atoms) having an average diameter of $\sim$3.2 Å and with up to 4 H_2 molecules incorporated along the principal axis of the tube $[(H_2)_4@(H_2)_{36}@C_{110}]$. In addition, notice that, for 40 H_2 encapsulated hydrogens (that define the maximum storage capacity), the positions of the carbon atoms located at the capped ends are almost unchanged, being practically independent of the density of the stored hydrogens (compare insets of Figs. 6 and 7). On the other hand, the C— C bonds located at the center are now expanded by $\sim$11%, locally increasing the average diameter of the C_{110} capsule. Actually, adding one more hydrogen molecule to this last structure results in the rupture of some C— C bonds located precisely around the center of the tube, allowing the possibility for some H_2 molecules to leak out of the structure.

In Fig. 8(a) we show results for the average repulsive interactions between H_2 molecules, $E_{rep}(H_2\text{-}H_2)$, as well as for those between the H_2 molecules and the fullerene wall, E_{rep}(wall-H_2), as a function of the number of the stored hydrogens. Following the authors of Ref. 18 $E_{rep}(H_2\text{-}H_2)$ is calculated from

$$E_{rep}(H_2\text{-}H_2) = E_t(H_n) - n_{H_2} E_{H_2}, \tag{3.2}$$

and similarly that between the tube wall and H_2 molecules is calculated by

$$E_{rep}(\text{wall-H}_2) = E_t(\text{SWNT} + \text{H}_n) - E_t(\text{SWNT}) - E_t(\text{H}_n), \tag{3.3}$$

where $E_t(\text{H}_n)$ is the total energy of H_n in the SWNT and n_{H_2} and E_{H_2} are the number of gaseous H_2 molecules and the total energy of a single gaseous H_2 molecule, respectively.

From Fig. 8(a) we note that both $E_{rep}(\text{H}_2\text{-H}_2)$ and $E_{rep}(\text{wall-H}_2)$ are almost the same for low and intermediate concentration regimes ($4 \rightarrow 24$ H_2 molecules), following an almost linear dependence as a function of the number of stored hydrogens. However, note that for higher H_2 up takes, H_2-H_2 repulsive energies become larger than those corresponding to wall-H_2 which, together with the nonuniform distribution of the H_2 molecules, increases the dimensions of the carbon structure (see Figs. 6 and 7) eventually breaking various of the C— C bonds located at the center of the cylindrical cavity (see discussion above). At the maximum storage capacity (40 H_2) we have found that the average repulsive interaction between H_2 molecules is 1.26 eV/H_2 and that between the tube wall and the encapsulated hydrogens is 1.05 eV/H_2, and energy ordering that agrees with the one found by the authors of Ref. 18 that have estimated $E_{rep}(\text{H}_2\text{-H}_2) = 0.89$ eV/H_2 and $E_{rep}(\text{wall-H}_2) = 0.7$ eV/H_2 for similar encapsulating cavities at high H_2 uptakes. In fact, notice that the same energy difference between the two repulsive interactions (~ 0.2 eV/H_2) is obtained in both works.

It is interesting to relate the results shown in Figs. 4–7 and 8(a) with the behavior of the average distance $\langle R_{\text{H}_2-\text{H}_2} \rangle$ between the encapsulated H_2 molecules shown in Fig. 8(b). This is particularly important in order to explain fine details of Fig. 8(a), like for example the energy crossings between $E_{rep}(\text{H}_2\text{-H}_2)$ and $E_{rep}(\text{wall-H}_2)$ observed at 26 and 28 H_2, as well as to reveal the strong correlation of $\langle R_{\text{H}_2\text{-H}_2} \rangle$ with the various structural transformations already seen in Figs. 4 and 5 as a function of the density of stored hydrogens. From Fig. 8(b) we note that the previously discussed $1\text{D} \rightarrow 2\text{D} \rightarrow 3\text{D}$ structural transitions (see Fig. 4) are clearly reflected in the abrupt variations of $\langle R_{\text{H}_2-\text{H}_2} \rangle$ (sizable global expansions and contractions of the molecular clusters) for 4, 5, and 7 H_2. Moreover, note that the existence of only hollow molecular assemblies ($12 \rightarrow 22$ H_2) is reflected in an almost increasing linear behavior of $\langle R_{\text{H}_2-\text{H}_2} \rangle$. However, upon incorporation of the first H_2 molecule along the z axis of the cavity $[\text{H}_2@(\text{H}_2)_{23}@\text{C}_{110}]$ a deviation from the linear behavior starts to develop (see results for 24 H_2). In fact, for 26 H_2 where now 3 H_2 molecules are placed along the z axis $[(\text{H}_2)_3@(\text{H}_2)_{23}@\text{C}_{110}]$, $\langle R_{\text{H}_2-\text{H}_2} \rangle$ clearly decreases its value. Concerning the evolution of the repulsive interactions [Fig. 8(a)] around this concentration regime we note that, for 26 H_2, $E_{rep}(\text{H}_2\text{-H}_2)$ also lowers its value, even with respect to the wall-H_2 repulsion. In this case, due to the formation of an axial phase, the density of hydrogens does not increase on the surface of the molecular cluster (which represents the major contribution to the H_2-H_2 repulsion), leading thus to reduced values of $E_{rep}(\text{H}_2\text{-H}_2)$ and to an average contraction of the molecular cluster as a whole [see Fig. 8(b)]. Interestingly, for 28 H_2, two of the three molecules located along the z axis in the last case migrate back to the surface of the molecular cluster, leaving again only one H_2 molecule asymmetrically placed along the z axis $[\text{H}_2@(\text{H}_2)_{27}@\text{C}_{110}]$. This obviously increases the density of hydrogens on the surface of the molecular assembly (from 23 to 27 H_2), a fact that also increases the value of $E_{rep}(\text{H}_2\text{-H}_2)$ [see Fig. 8(a)], inducing as a consequence an expansion in the molecular cluster [see Fig. 8(b)] as well as in various of the C— C bonds of the encapsulating cavity. From these results we can thus conclude that, as physically expected, the energetics and structural rearrangements presented in the figures result from a delicate balance between the electronic and geometrical details present in the particles.

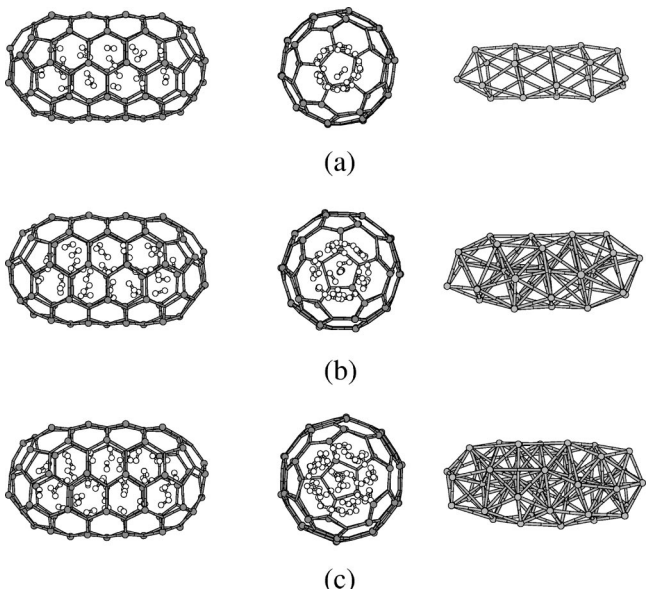

FIG. 9. Calculated (MNDO) lowest-energy structures (left column), side view of the equilibrium configurations (central column), and the respective spatial distribution of the center of masses of the encapsulated hydrogens (right column) for (a) $(\text{H}_2)_{20}@\text{B}_{55}\text{N}_{55}$, (b) $(\text{H}_2)_{30}@\text{B}_{55}\text{N}_{55}$, and (c) $(\text{H}_2)_{41}@\text{B}_{55}\text{N}_{55}$ fullerenes. In the first two columns B atoms are represented as balls.

2. Hydrogen storage in a (5,5) BN capsule

Hydrogen storage in noncarbon fullerenes is also interesting to analyze, mainly in single-wall BN tubes and related fullerene structures (multiwall nanotubes, bundles, etc)[22,47] that have shown also interesting electronic properties and remarkable stability. Consequently, we have decided to perform also a systematic study of the hydrogen storage behavior in a finite-(5,5) 110-atom BN capsule. In Fig. 9 we show as representative results the equilibrium configurations found for 20, 30, and 41 H_2 molecules encapsulated in a 110-atom BN structure, the latter value defining the maximum storage capacity of the fullerene cavity. From the figure we note that, in agreement with the corresponding pure carbon arrangements (see Fig. 5), hollow helicoidal tubelike molecular assemblies together with axial configurations (i.e., H_2 molecules incorporated along the z axis of the cavity) are also obtained. However, by looking at the precise details of the

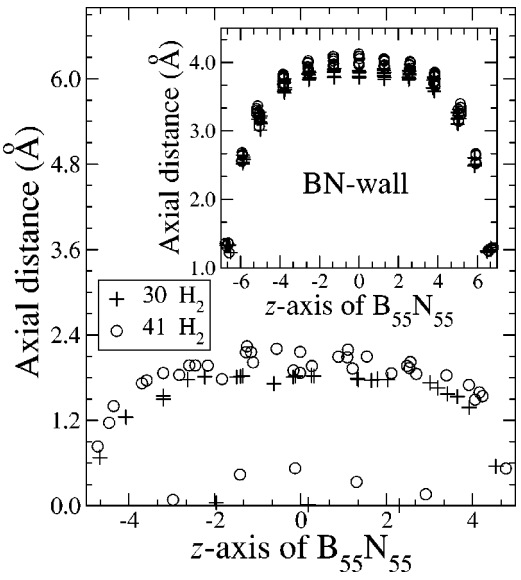

FIG. 10. Axial distance (in Å) of each one of the center of masses of the encapsulated H_2 in a $B_{55}N_{55}$ fullerene with respect to the principal symmetry axis of the cavity (z axis) for 30 H_2 (plus) and 41 H_2 (open circles). In the inset, we show similar results but for each one of the B and N atoms of the BN capsule.

spatial distribution of the stored hydrogens as well as to the orientational distribution of the molecular axes in both C_{110} (Fig. 5) and $B_{55}N_{55}$ cages, we can observe sizable differences in the structures of the various molecular assemblies. This is most notable at high H_2 densities where an interesting additional structural transition within the BN cavity has been obtained. This fact is more clearly seen from Fig. 10 where we plot the distribution of distances of the center of masses of 30 and 41 encapsulated hydrogen molecules with respect to the principal symmetry axis of the tube (z axis). From the figure we note that the slightly larger available space provided by the BN structure (actually we calculate an average nearest-neighbor bond length of 1.49 Å for the empty BN capsule, being $\sim$3.5% larger than that obtained for the C_{110}) allows a $1D[(H_2)_4@(H_2)_{36}@B_{55}N_{55}] \rightarrow 2D[(H_2)_5@(H_2)_{36}@B_{55}N_{55}]$ structural phase transition for the axial array of H_2 molecules (see results for 41 H_2 in Fig. 10), being exactly the same as that observed between Figs. 4(a) to 4(b). Consequently, for bigger encapsulating cavities it is thus reasonable to expect, and actually it has been already shown for SWCNT's with different diameters,[18] the gradual stabilization of 2D and 3D configurations inside the H_2 molecular cluster, resulting in the formation of various concentric assemblies of cylindrical shape.

From the inset of Fig. 10 we note also that, when compared with the distribution of C atoms shown in the insets of Figs. 6 and 7, a larger dispersion in the positions of B and N units of the cage with respect to the z axis is obtained. A similar effect is already seen in the empty structure where, as a consequence of the different size of B and N atoms, the walls of the optimized encapsulating cavity are found to be slightly undulating, the B atoms moving inward but the N atoms move outward. In addition, we note that, as in the C capsule, the position of the atoms located at the central region of the BN tube are the ones suffering the largest radial expansions, due to the also highly anisotropic repulsive interactions between the different chemical species present in the system. This result also confirms the previously demonstrated fact that nanotubes are extremely rigid to distortions along the tube axis, while they are very flexible to be deformed in a direction perpendicular to the axis. It is important to comment that, in the particular case of empty BN and BC_3 nanotubes, recent *ab initio* calculations[48] have shown that this type of radial deformations can lead to strong variations in the band gap of the structures, a result that can be very useful for optical applications in the visible range. In fact, following the above work we have noted that, when comparing the energy-level distribution of an empty BN capsule with the one containing 41 H_2 molecules (which is considerably radially deformed), we have found a reduction of $\sim$10% in the HOMO-LUMO energy gap. Actually, a similar result has been also obtained at hydrogen-containing pure carbon nanotubes for which also a sizable reduction in the HOMO-LUMO energy difference is observed ($\sim$13%) for the largest radially deformed structure [see Fig. 5(c)] when compared to the calculated value for the empty C_{110} cavity.

C. Influence of the capped ends

As already stated in Sec. II B, carbon nanotubes as produced are capped, among other ways, with hemispherical fullerene domes containing six pentagons required to produce closure. However, if using capillarity techniques, nanotubes must have open ends to allow adsorption of small molecules inside the tubes. As is well known, oxidation procedures[49] have been used to create open-ended structures by breaking some of the C—C bonds at the closed caps which are more susceptible because of the presence of the highly reactive five-membered rings. Then, under heavy gas exposure, small molecules can be adsorbed at the interior of the tube at moderate temperatures and pressures and finally, it is necessary to effectively sealed the end of the tube. A possible procedure to realize this last crucial step may be the attachment of polymers or small molecules to the unsaturated C atoms located at the open-ended region of the tube. In this respect, the size, ring structure, and flexibility of the siloxane molecules $[SiO]_N$ makes them very appropriate to achivied this goal. In this section, we will analyze then the adsorption of a single cyclopentasiloxane molecule $[SiO]_5$ to the open end of a (5,5) 110-atom carbon nanotube. We will determine the structural properties and stability of the $[SiO]_5$-fullerene compound and his implications in the hydrogen storage capacity of the carbon structure.

As we show in Fig. 11(a), at the MNDO level, $[SiO]_5$ as a free molecule has a ringlike two-dimensional structure with Si—O bond lengths of 1.61 Å. However, when attached to the open end of a (5,5) carbon nanotube [see Fig. 11(b)], with an adsorption energy of 4.9 eV, it develops a kind of ''puckered-type'' of structure where the O atoms do not bond to the carbon cage and move outside the cavity, forming a weaker Si—O bond (1.64 Å). On the other hand, the Si atoms are strongly bonded to the carbon structure with nearest-neighbor Si—C distances of 1.8 Å, being of the or-

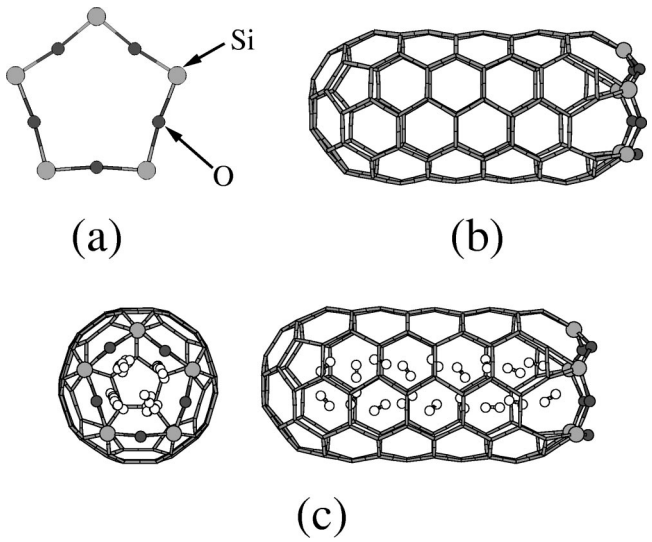

FIG. 11. Calculated (MNDO) lowest-energy structures for (a) a single cyclopentasiloxane molecule, (b) the $C_{110}[SiO]_5$ capsule, (c) and for the $(H_2)_{18}@C_{110}[SiO]_5$ system.

der of the ones found in organic molecules (1.8–1.9 Å).[50] Despite the equilibrium configuration does not effectively sealed the fullerene cavity, it is clear that a larger energy barrier height (when compared with the open structure) needs to be overcome for some H_2 molecules to leak out of the structure.

In Fig. 11(c), we show the lowest-energy configuration for the $(H_2)_{18}@C_{110}[SiO]_5$ compound. In this respect, it is important to comment that several initial configurations and densities of encapsulated hydrogens were considered (up to 25 H_2), however, in all cases we have observed that for the $C_{110}[SiO]_5$ fullerene shown in Fig. 11(b) only 18 hydrogen molecules can exist in the inside of the tube. In addition, by looking at the side view in Fig. 11(c), we clearly see the stabilization of four linear arrays of H_2 molecules, a configuration that obviously differs from the hollow molecular assembly observed in Fig. 5(a) for the same number of encapsulated hydrogens. As in the case of spheroidal fullerenes, this result also reveals the importance of the precise geometrical details of the encapsulating cavity on the form of the stored hydrogens.

Interestingly, for a number of encapsulated hydrogens larger than 18, a ''diffusion'' process is observed through the $[SiO]_5$ ring which gradually reduces the number of H_2 molecules in the tube, and that actually stops when the H_2-H_2 and wall-H_2 repulsive interactions present in the system are not enough to overcome the energy barrier height imposed by the cyclic $[SiO]_5$ molecule attached to one of the ends. This behavior seems to provide a controlled way to store precise amounts of gases, a fact that could be of fundamental importance when specific doses need to be supplied. Obviously, by reducing the ring size of the molecular termination, a larger energy barrier will be imposed for the encapsulated H_2, a fact that will increase in a controlled way the storage capacity of the fullerene compound.

IV. SUMMARY AND CONCLUSIONS

In this work we have presented a systematic study, by combining semiempirical and DFT approaches, of the hydrogen storage behavior in spheroidal C_{60} and C_{82}, as well as in cylindrical C_{110} and $B_{55}N_{55}$ fullerenes. Our results have shown that, as a function of the size and symmetry of the fullerene cavity, as well as of the density of stored molecules, the encapsulated hydrogens form a wide variety of molecular clusters. In agreement with well-known phenomena in molecular solids, we have found ordered→disordered structural rearrangements induced by rotational reorientation transitions of the individual H_2 molecules. In our tubelike configurations, we relate the bond-breakage mechanism of the fullerene network to the development of a nonuniform hydrogen accommodation along the tubes, driven the highly anisotropic repulsive interactions between the different chemical species (H_2-H_2 and wall-H_2) present in the systems. From our calculations we have found that, with increasing the number of stored hydrogens, tubes are mainly radially deformed, a fact that leads to sizable reductions in the HOMO-LUMO energy difference, increasing thus the conductivity of the structures. Finally, by attaching a single cyclopentasiloxane molecule to an open end of a carbon nanotube it seems to be possible to develop a controlled way to store precise doses of gases in the inside of carbon nanotubes.

ACKNOWLEDGMENTS

The authors would like to acknowledge the financial support from CONACyT (México) for Grant Nos. 129747 and J32084-E.

[1] M. Endo, K. Takeuchi, K. Kobori, K. Takahashi, H.W. Kroto, and A. Sarkar, Carbon **33**, 874 (1995).

[2] P.M. Ajayan and S. Iijima, Nature (London) **361**, 333 (1993); C.N.R. Rao, R. Seshadri, A. Govindaraj, and R. Sen, Mater. Sci. Eng., R. **15**, 209 (1995); B.C. Sathishkumar, A. Govindaraj, J. Mofokeng, G.N. Subbanna, and C.N.R. Rao, J. Phys. B **29**, 4925 (1996); T.W. Odom, J.L. Huang, C.L. Cheung, and C.M. Lieber, Science **290**, 1549 (2000).

[3] A.F. Hebard, M.J. Rosseinsky, R.C. Haddon, D.W. Murphy, S.H. Glarum, T.T.M. Palstra, A.P. Ramirez, and A.R. Kortan, Nature (London) **350**, 600 (1991).

[4] C. Prados, P. Crespo, J.M. González, A. Hernando, J.F. Marco, R. Gancedo, N. Grobert, M. Terrones, R.M. Walton, and H.W. Kroto, Phys. Rev. B **65**, 113405 (2002).

[5] C. Liu, Y.Y. Fan, M. Liu, H.T. Cong, H.M. Cheng, and M.S. Dresselhaus, Science **286**, 1127 (1999); C.C. Ahn, Y. Ye, B.V. Ratnakumar, C. Witham, R.C. Bowman, and B. Fultz, Appl. Phys. Lett. **73**, 378 (1998); P. Chen, X. Wu, J. Lin, and K.L. Tan,

Science **285**, 91 (1999); R.C. Gordillo, J. Boronat, and J. Casulleras, Phys. Rev. Lett. **85**, 2348 (2000).

[6] X. Lu, R. O. Loutfy, E. Veksler, and J. C. Wang, in *Symposium on Recent Advances in the Chemistry and Physics of Fullerenes and Related Materials*, edited by K. M. Kadish and R. S. Rouff (Electrochemical Society, Pennington, NJ, 1998).

[7] A.C. Dillon, K.M. Jones, T.A. Bekkedahl, C.H. Kiang, D.S. Bethune, and M.J. Heben, Nature (London) **386**, 377 (1997).

[8] A. Chambers, C. Park, T.K. Baker, and N.M. Rodriguez, J. Phys. Chem. B **108**, 4523 (1998).

[9] Q. Wang and J.K. Johnson, J. Chem. Phys. **110**, 577 (1999); F. Darkrim and D. Levesque, *ibid.* **109**, 4981 (1998).

[10] C.C. Ahn, Y. Ye, B.V. Ratnakumar, C. Witham, R.C. Bowman, Jr., and B. Fultz, Appl. Phys. Lett. **73**, 3378 (1998).

[11] Y. Ye, C.C. Ahn, C. Witham, B. Fultz, J. Liu, A.G. Rinzler, D. Colbert, K.A. Smith, and R.E. Smalley, Appl. Phys. Lett. **74**, 2307 (1999).

[12] S. Hynek, W. Fuller, and J. Bentley, Int. J. Hydrogen Energy **14**, 437 (1998).

[13] F. Darkrim and D. Levesque, J. Phys. Chem. B **104**, 6773 (2000).

[14] R. Smith, K. Beardmore, and J. Belbruno, J. Chem. Phys. **111**, 9227 (1999).

[15] Y. Ma, Y. Xia, M. Zhao, R. Wang, and L. Mei, Phys. Rev. B **63**, 115422 (2001).

[16] Z. Wan, J.F. Christian, and S.L. Anderson, J. Phys. Chem. **96**, 3344 (1992); Z. Wan, J.F. Christian, Y. Basir, and S.L. Anderson, *ibid.* **99**, 5858 (1993).

[17] G. Stan and M.W. Cole, J. Low Temp. Phys. **110**, 539 (1998); G. Stan and M.W. Cole, Surf. Sci. **395**, 280 (1998); M. Rzepka, P. Lamp, and M. A. de la Casa-Lillo, J. Phys. Chem. **102**, 10894 (1998).

[18] S.M. Lee and Y.H. Lee, Appl. Phys. Lett. **76**, 2877 (2000).

[19] V.V. Simonyan, P. Diep, and K. Johnson, J. Chem. Phys. **111**, 9778 (1999).

[20] A.M. Vidales, V. Crespi, and M. Cole, Phys. Rev. B **58**, R13 426 (1998).

[21] M. Hodak and L.A. Girifalco, Phys. Rev. B **64**, 035407 (2001).

[22] N.G. Chopra, R.J. Luyken, K. Cherrey, V.H. Crespi, M.L. Cohen, S.G. Louie, and A. Zettl, Science **269**, 996 (1995); D. Golberg, Y. Bando, K. Kurashima, and T. Sato, Solid State Commun. **116**, 1 (2000); E. Bengu and L.D. Marks, Phys. Rev. Lett. **86**, 2385 (2001).

[23] M.J.S. Dewar and W. Thiel, J. Am. Chem. Soc. **99**, 4899 (1977); **99**, 4907 (1977).

[24] A. Becke, Phys. Rev. A **38**, 3098 (1988); C. Lee, W. Yang, and R.G. Parr, Phys. Rev. B **36**, 785 (1988).

[25] D. Bakowies and W. Thiel, J. Am. Chem. Soc. **113**, 3704 (1991).

[26] K. Hedberg, L. Hedberg, D.S. Bethune, C.A. Brown, H.C. Dorn, R.D. Johnson, and M. de Vries, Science **254**, 410 (1991).

[27] M. Häser, J. Almlöf, and G.E. Scuseria, Chem. Phys. Lett. **181**, 497 (1991).

[28] H.P. Lüthi and J. Almlöf, Chem. Phys. Lett. **135**, 357 (1987).

[29] J. de Vries, H. Steger, B. Kanke, C. Manzel, B. Weisser, W. Kamke, and I.V. Hertel, Chem. Phys. Lett. **188**, 159 (1992).

[30] U. Zimmermann, A. Burkhardt, N. Malinowsky, U. Näher, and T.P. Martin, J. Chem. Phys. **101**, 2244 (1994).

[31] D.L. Strout, R.L. Murry, C. Xu, W.C. Eckhoff, G.K. Odom, and G.E. Scuseria, Chem. Phys. Lett. **214**, 576 (1993).

[32] M. J. Frisch, G. W. Trucks, H. B. Schlegel, G. E. Scuseria, M. A. Robb, J. R. Cheeseman, V. G. Zakrzewski, J. A. Montgomery, Jr., R. E. Stratmann, J. C. Burant, S. Dapprich, J. M. Millam, A. D. Daniels, K. N. Kudin, M. C. Strain, O. Farkas, J. Tomasi, V. Barone, M. Cossi, R. Cammi, B. Mennucci, C. Pomelli, C. Adamo, S. Clifford, J. Ochterski, G. A. Petersson, P. Y. Ayala, Q. Cui, K. Morokuma, D. K. Malick, A. D. Rabuck, K. Raghavachari, J. B. Foresman, J. Cioslowski, J. V. Ortiz, A. G. Baboul, B. B. Stefanov, G. Liu, A. Liashenko, P. Piskorz, I. Komaromi, R. Gomperts, R. L. Martin, D. J. Fox, T. Keith, M. A. Al-Laham, C. Y. Peng, A. Nanayakkara, M. Challacombe, P. M. W. Gill, B. Johnson, W. Chen, M. W. Wong, J. L. Andres, C. Gonzalez, M. Head-Gordon, E. S. Replogle, and J. A. Pople, GAUSSIAN 98, REVISION A.9, (Gaussian, Pittsburgh PA, 1998.

[33] W.J. Hehre, R.F. Stewart, and J.A. Pople, J. Chem. Phys. **51**, 2657 (1969); J.B. Collins, P.v.R. Schleyer, J.S. Binkley, and J.A. Pople, *ibid.* **64**, 5142 (1976).

[34] J.S. Binkley, J.A. Pople, and W.J. Henre, J. Am. Chem. Soc. **102**, 939 (1980); M.S. Gordon, J.S. Binkley, J.A. Pople, W.J. Pietro, and W.J. Henre, *ibid.* **104**, 2797 (1982).

[35] K. Kobayashi and N. Kurita, Phys. Rev. Lett. **70**, 3542 (1993), and references therein.

[36] J.H. Weaver, J.L. Martins, T. Komeda, Y. Chen, T.R. Ohno, G.H. Kroll, N. Troullier, R.E. Haufler, and R.E. Smalley, Phys. Rev. Lett. **66**, 1741 (1991).

[37] R.W. Lof, M.A. van Veenendaal, B. Koopmans, H.T. Jonkman, and G.A. Sawatzky, Phys. Rev. Lett. **68**, 3924 (1992).

[38] B.V. Reddy, S.N. Khanna, and B.I. Dunlap, Phys. Rev. Lett. **70**, 3323 (1993).

[39] M. Pederson, K.A. Jackson, and L.L. Boyer, Phys. Rev. B **45**, 6919 (1992).

[40] A. Rubio, J. Corkill, and M.L. Cohen, Phys. Rev. B **49**, 5081 (1994); X. Blase, A. Rubio, S.G. Louie, and M.L. Cohen, Europhys. Lett. **28**, 335 (1994).

[41] G. Torchet, M.-F. de Feraudy, A. Boutin, and A.H. Fuchs, J. Chem. Phys. **105**, 3671 (1996).

[42] A. Boutin, J.B. Maillet, and A.H. Fuchs, J. Chem. Phys. **99**, 9944 (1993).

[43] F. Seitz, *Modern Theory of Solids* (McGraw-Hill, New York, 1940).

[44] Y.F. Yin, T. Mays, and B. McEnaney, Langmuir **16**, 10521 (2000).

[45] I.A. Khan and K.G. Ayappa, J. Phys. Chem. **109**, 4576 (1998).

[46] M. Cháavez-Páez, M. Medina-Noyola, and M. Valdéz-Covarrubias, Phys. Rev. E **62**, 5179 (2000).

[47] A. Loiseau, F. Willaime, N. Demoncy, G. Hug, and H. Pascard, Phys. Rev. Lett. **76**, 4737 (1996); M. Terrones, W.K. Hsu, H. Terrones, Z.P. Zhang, S. Ramos, I.P. Hare, R. Castillo, K. Prasides, A.K. Cheeetham, H.W. Kroto, and D.R.M. Walton, Chem. Phys. Lett. **259**, 568 (1996).

[48] Y.H. Kim, K.J. Chang, and S.G. Louie, Phys. Rev. B **63**, 205408 (2001).

[49] S.C. Tsang, Y.K. Chen, P.J.F. Harris, and M.L.H. Green, Nature (London) **372**, 159 (1994).

[50] J. H. Callomon, E. Hirota, T. Iijima,K. Kuchitsu, and W.J. Lafferty, in *Structure Data of Free Polyatomic Molecules*, edited by K. H. Hellwege and A. M. Hellwege, Landolt Börstein Vol. New Series II/15 (Springer-Verlag, Berlin-Heidelberg, 1987).